



HAL
open science

Optical data storage in photosensitive glasses and spin state transition compounds

Matthieu Bellec, Lionel Canioni, Arnaud Royon, Bruno Bousquet, Jérôme Degert, Eric Freysz, Thierry Cardinal, Jean-François Letard

► **To cite this version:**

Matthieu Bellec, Lionel Canioni, Arnaud Royon, Bruno Bousquet, Jérôme Degert, et al.. Optical data storage in photosensitive glasses and spin state transition compounds. Florin Balasa. Data Storage, InTech, pp.33-51, 2010, 978-953-307-063-6. 10.5772/8874 . hal-00609299

HAL Id: hal-00609299

<https://hal.science/hal-00609299>

Submitted on 13 Jul 2023

HAL is a multi-disciplinary open access archive for the deposit and dissemination of scientific research documents, whether they are published or not. The documents may come from teaching and research institutions in France or abroad, or from public or private research centers.

L'archive ouverte pluridisciplinaire **HAL**, est destinée au dépôt et à la diffusion de documents scientifiques de niveau recherche, publiés ou non, émanant des établissements d'enseignement et de recherche français ou étrangers, des laboratoires publics ou privés.

Optical data storage in photosensitive glasses and spin state transition compounds

Matthieu Bellec, Lionel Canioni, Arnaud Royon, Bruno Bousquet,
Jérôme Degert and Eric Freysz

*Centre de Physique Moléculaire Optique et Hertzienne (CPMOH), University of Bordeaux
France*

Thierry Cardinal and Jean-François Létard

*Institut de Chimie de la Matière Condensée de Bordeaux (ICMCB), University of Bordeaux
France*

1. Introduction

Up to now, the common media for optical data storage are the discs (blue ray technology for example). However, by definition, this technology is limited to two dimensions. The necessity for increasing data storage capacity requires the use of three-dimensional (3D) optically based systems. One of the methods for 3D optical data storage is based on volume holography. The physical mechanism is photochromism, which is defined as a reversible transformation of a single chemical species between two states that have different absorption spectra and refractive indices. This allows for holographic multiplexing recording and reading, such as wavelength (Rakuljic et al., 1992), angular (Mok, 1993), shift (Psaltis et al., 1995) and phase encoding. Another promising 3D optical data storage system is the bit-by-bit memory at the nanoscale (Li et al., 2007). It is based on the confinement of multi-photon absorption to a very small volume because of its nonlinear dependence on excitation intensity. This characteristic provides an income for activating chemical or physical processes with high spatial resolution in three dimensions. As a result there is less cross talk between neighbouring data layers. Another advantage of multi-photon excitation is the use of infrared (IR) illumination, which results in the reduction of scattering and permits the recording of layers at a deep depth in a thick material. Two-photon 3D bit recording in photopolymerizable (Strickler & Webb, 1991), photobleaching (Pan et al., 1997; Day & Gu, 1998) and void creation in transparent materials (Jiu et al., 2005; Squier & Muller, 1999) has been demonstrated with a femtosecond laser. Recording densities could reach terabits per cubic centimeter. Nevertheless, these processes suffer from several drawbacks. The index modulation associated with high bit density limits the real data storage volume due to light scattering. The fluorescence can limit the data transfer rate and the lifetime of the device.

Thanks to various available compositions, ease of implementation, stability and transparency, both organic and inorganic materials are convenient for 3D data storage. To be good candidates for 3D optical data storage, these materials must satisfy several norms

for the storing and the reading: Resistance to ageing due to temperature and recurrent reading. Moreover, high-speed response for high rate data transfer, no optically scattering for multilayer storage, erasure and eventually record with a grayscale to increase the data density could be incontrovertible advantages.

Here, we present two particular media: A photosensitive glass (zinc phosphate glass containing silver) in which the contrast mechanism is neither a change in refractive index nor a change in absorption, but a change in the third-order susceptibility ($\chi^{(3)}$) induced by femtosecond laser irradiation (Canioni et al., 2008); and a spin state transition material.

2. Photosensitive glass

2.1. Data storage medium: Photosensitive zinc phosphate glass containing silver

Glasses with composition $40\text{P}_2\text{O}_5\text{-}4\text{Ag}_2\text{O-}55\text{ZnO-}1\text{Ga}_2\text{O}_3$ (mol%) were prepared for 3D data storage using a standard melt quench technique. $(\text{NH}_4)_2\text{HPO}_4$, ZnO, AgNO_3 and Ga_2O_3 in powder form were used as raw materials and placed with the appropriate amount in a platinum crucible. A heating rate of about $1^\circ\text{C}\cdot\text{min}^{-1}$ has been conducted up to 1000°C . The melt was then kept at this last temperature (1000°C) from 24 to 48 hours. Following this step, the liquid was poured into a brass mold after a short increase of the temperature at 1100°C in order to access the appropriate viscosity. The glass samples obtained were annealed at 320°C (55°C below the glass transition temperature) for 3 hours, cut (0.5 to 1 mm-thick) and optically polished. The glass possesses an absorption cut-off wavelength at 280 nm (due to the silver ions associated absorption band around 260 nm) and emits fluorescence mainly around 380 nm when excited at 260 nm. This intrinsic fluorescence is due to Ag^+ isolated in the glass (Belharouak et al., 1999).

The processed glass is highly photosensitive and was originally developed as a gamma irradiation dosimeter (Schneckenburger et al., 1981; Dmitryuk et al., 1996). Following exposure to gamma rays, the glass presents a broad UV absorption band, and when excited by UV radiation, emits homogeneous fluorescence which intensity is proportional to the irradiation dosage. This fluorescence is attributed to the presence of silver nanoclusters.

2.2. Silver nanoclusters formation following IR femtosecond irradiation

When an IR femtosecond laser is focused inside the photosensitive glass, a nonlinear multiphoton interaction occurs (in this case 4-photon-absorption) at the vicinity of the focal volume. Photoelectrons are ejected from the valence to the conduction band of the glass (Jones & Reiss, 1977; Stuart et al., 1996; Keldysh, 1965). In a similar manner to the mechanism utilized in a dosimeter (Schneckenburger et al., 1981; Dmitryuk et al., 1996), the released electrons are trapped within a few picoseconds by silver Ag^+ ions to form silver Ag^0 atoms. Then, due to the high laser repetition rate, the accumulation of the deposited laser energy increases the local temperature leading to the Ag^0 diffusion. Mobile Ag^0 atoms are trapped by the Ag^+ ions to form silver clusters Ag_m^{x+} with the number of atoms $m < 10$ and the ionization degree x . Since this is produced by a highly nonlinear interaction, the silver nanoclusters can be distributed in 3D inside the glass in an area that is smaller than the laser beam diameter (Sun et al., 2001). More details on the silver nanoclusters distribution in this glass can be found in (Bellec et al., 2009). The photo-induced silver nanoclusters have characteristic properties well adapted for the 3D optical data storage.

2.3. Silver nanoclusters spectral and optical properties

The photosensitive glass is irradiated using a femtosecond laser source emitting 440 fs, 9 MHz repetition rate pulses at 1030 nm. The laser mode is TEM₀₀, and the output polarization is TM. The maximum output average power is close to 6 W, which results in a maximum energy per pulse of 600 nJ. Acousto-optic filtering permits the tuning of the pulse energy and the repetition rate for perfect control of the accumulated effect. The femtosecond laser is focused using a reflective 36× objective with a 0.52 numerical aperture (NA) (working distance 15 mm) to a depth of 200 μm in the glass. The beam waist is estimated to be 1 μm. Spectroscopic properties (*i.e.* absorption and emission spectra) of the silver nanoclusters are shown in Fig 1. A transmission confocal setup, with a 36× - 0.52 NA reflective objective, is used for spectroscopy. A UV diode emitting at 405 nm with an appropriate emission filter, and a white light source are used to obtain emission and absorption spectra. All spectra are measured using a spectrometer equipped with a CCD camera. Figure 1(a) shows the absorbance difference between the irradiated region (experimental conditions: Irradiance $I = 6 \text{ TW}\cdot\text{cm}^{-2}$; Number of pulses $N = 10^6$) and the non-irradiated region. An absorption band appears at 345 nm. The emission spectrum of the fluorescent species when excited in the UV is presented in Fig. 1(b). A wide band centered at 580 nm is observed. These spectral properties can be attributed to the photoinduced silver nanoclusters (Dmitryuk et al., 1996; Dai et al., 2007).

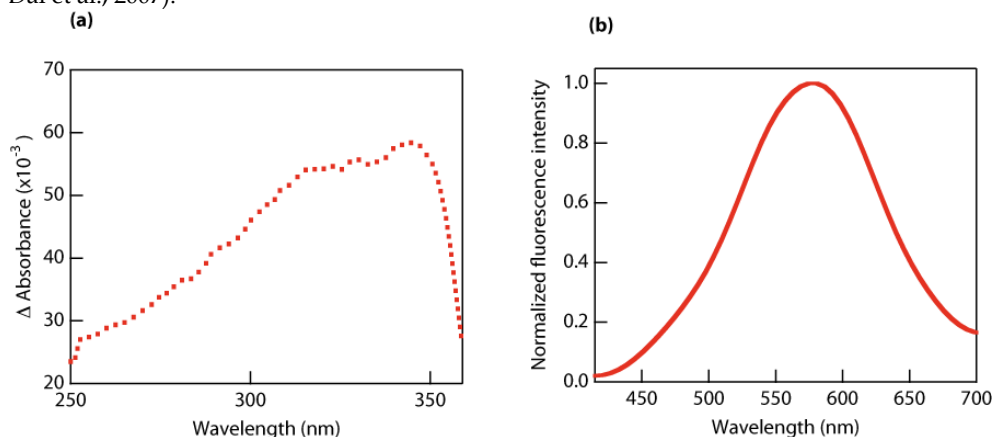


Fig. 1. (a) Differential absorbance spectrum between the irradiated and non-irradiated regions; (b) Emission spectrum (excitation wavelength, 405 nm) of the irradiated region. Experimental laser irradiation conditions: $I = 6 \text{ TW}\cdot\text{cm}^{-2}$, $N = 10^6$. Differential absorbance and emission spectra are assigned to laser induced Ag clusters.

The optical properties of the silver nanoclusters are studied for different irradiation conditions by white light, epifluorescence and third-harmonic generation (THG) microscopy. Thus, the glass is exposed to different irradiance levels (x axis) between $4 \text{ TW}\cdot\text{cm}^{-2}$ and $10 \text{ TW}\cdot\text{cm}^{-2}$ and a different number of pulses (y axis) from 10^2 to 10^6 , as shown on the experimental map sketch in Fig. 2(a). The sample is manipulated through patterning of bits with a bit spacing of 20 μm using a precision xyz stage. Epifluorescence microscopy are performed with commercial microscopes. A transmission confocal setup, with a 36× - 0.52 NA reflective objective, is used for THG data collection. The

THG signal is filtered from the fundamental one by an emission bandpass filter @ (350 ± 50) nm and is collected with a photomultiplier tube. In our case, THG is excited with the same laser at low energy 10 nJ/pulse, but practically, a cheaper laser, such as a femtosecond fiber laser, could be used. Indeed, with a minimum energy of 0.1 nJ and an irradiance of 10^{10} W.cm⁻² (corresponding to an average power of 10 mW with a 100 MHz repetition rate), more than one third-harmonic photon by incoming pulse can be detected (Brocas et al., 2004).

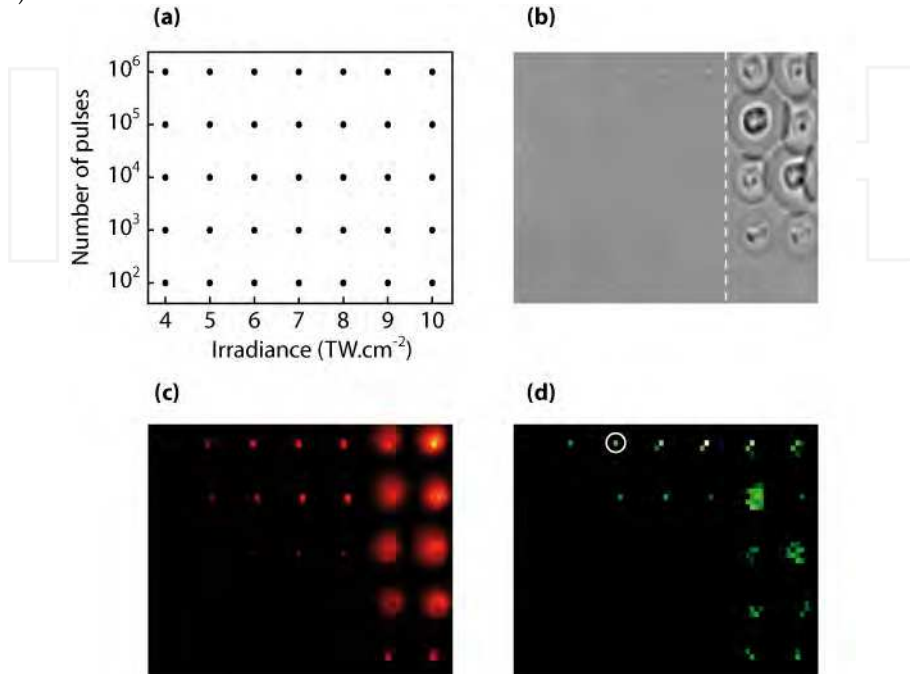


Fig. 2. Microscopy imaging of laser-induced species following the experimental map sketch. (a) x axis, laser irradiance; y axis, number of laser pulses, 6x5 bits pattern; spacing, 20 nm. (b) Epiwhite light microscopy image reveals linear refractive index modifications; vertical dashed line, damage threshold. (c) Epifluorescence microscopy image (excitation wavelength, 365 nm; emission filter, (610 ± 40) nm). (d) THG image (excitation wavelength, 1030 nm; emission filter, (350 ± 50) nm); encircled area, data storage irradiation conditions ($I = 6 \times \text{TW} \cdot \text{cm}^{-2}$, $N = 10^6$).

Transmission, fluorescence, and THG readout images of bits recorded with different irradiance levels and laser shots are presented in figures 2(b)–2(d). Figure 2(b) shows changes in refractive index. The damage threshold is achieved at an irradiance of 9 TW cm^{-2} , which is delimited by a vertical dashed line. At irradiances below this line, no apparent modifications are observed except for the high accumulated area in the upper part of Fig. 2(b). Nevertheless, in Fig. 2(c), we observe that fluorescence is obtained in regions where the refractive index is not modified. The same behavior is observed on the THG image in Fig. 2(d).

The THG image confirms that the induced Ag clusters absorb at 343 nm, corresponding to

the resonant third-harmonic of the laser wavelength. Indeed, a coherent third-harmonic signal could be generated by each center due to the resonant absorption. The irradiated region is in the weak absorption regime and allows an enhancement of the third harmonic signal (Shen, 1984; Barille et al., 2002). Moreover, the image contrast is proportional to $|\chi_R^{(3)} - \chi_{NR}^{(3)}|^2$, where $\chi_R^{(3)}$ and $\chi_{NR}^{(3)}$ are the third-order susceptibilities of the irradiated (resonant) and non-irradiated (nonresonant) regions (Barille et al., 2002). The signal is due to the electronic contribution to $\chi^{(3)}$, since only the electronic polarization is able to quickly respond to a high frequency all-optical field excitation. Therefore, at the vicinity of the nonlinear interface between the Ag clusters and the glass matrix, a coherent third-harmonic signal can be generated under femtosecond laser excitation at 1030 nm.

Thus, as illustrated in Fig 3, the data can be stored inside the glass by femtosecond laser irradiation below the refractive index modification threshold. Thanks to thermal cumulative effects, stable Ag nanoclusters are created, giving rise to the formation of a nonlinear resonant interface (Fig. 3(a)). THG readout becomes possible using the same laser with less energy (Fig. 3(b)).

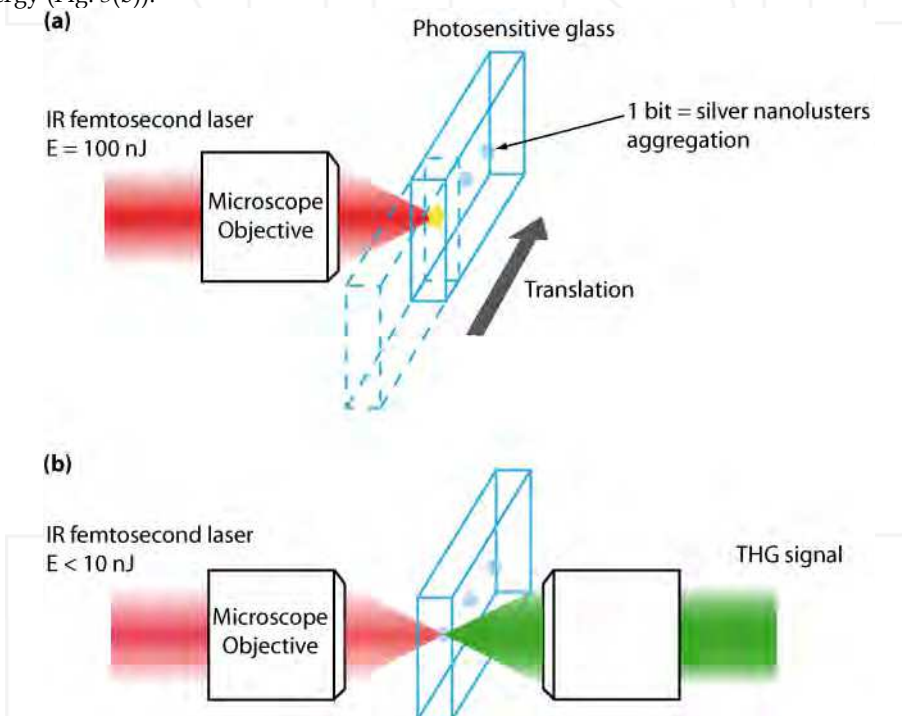


Fig. 3. Writing and reading processes. (a) Data are stored inside the photosensitive glass by focusing an IR femtosecond laser. 1 bit corresponds to a silver nanoclusters aggregation which presents no refractive index modifications. (b) Using the same laser with less energy, the third-harmonic signal can be collected.

2.4. Reading process by third-harmonic generation

To demonstrate the 3D optical data storage performance according to the principle

explained before, a 3D bit pattern embedded in the photosensitive glass is written and read by a THG imaging setup. To achieve a high bit density in the volume, the change in refractive index must be kept as low as possible to minimize the effect of scattering of the reading beam while the change in $\chi^{(3)}$ must be as high as possible. We choose to work below the damage threshold to minimize the refractive index modification and optimize creation of aggregates by the accumulated effect (the corresponding area is encircled in Fig. 2(d)). The sample is irradiated with a laser irradiance of $6 \text{ TW}\cdot\text{cm}^{-2}$ and with 10^6 pulses. Three layers of data are embedded 200 nm inside the sample. Each layer contains a pattern of 12×12 bits with a bit spacing of 3 nm. The letters U, B, and the numeral 1 (for University Bordeaux 1) are recorded in the first, second, and third layers, respectively, with a layer spacing of 10 nm in the z direction. As shown previously, the same laser is used for the reading procedure but with a lower irradiance. By scanning the sample in xyz through the focus, the three layers (U, B, and 1) are reconstructed and presented in Fig. 3.

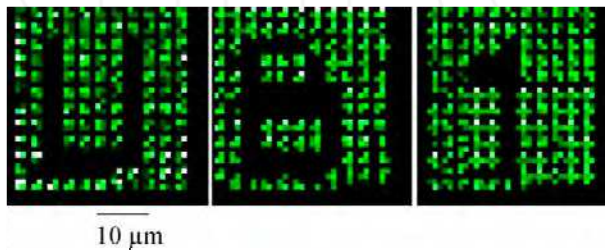


Fig. 4. THG readout of the three layers containing the bit patterns U, B, and 1, recorded in the bulk of the glass (bit spacing, 3 nm; layer spacing, 10 nm). Laser writing parameters: $I = 6 \text{ TW}\cdot\text{cm}^{-2}$, $N = 10^6$. The three THG images present high signal-to-noise ratio and no cross talk.

As expected by the THG mechanism, an image with high contrast and no cross talk is observed in Fig. 3. The main advantages of this technique compared to usual 3D data storage are no photobleaching, no change in linear refractive index, and therefore no scattering. Moreover, the THG signal is coherent and gives rise to a rather intense, directional, and less divergent beam with a high signal-to-noise ratio. Due to the fast THG response, the reading speed is limited only by the pulse duration.

2.5. Grayscale encoding

Fig. 2(d) shows that the THG signal depends on the number of pulses. This can be used to encode the information onto a grayscale. Using an acousto-optic modulator, the number of pulses is well controlled. As presented in the Fig. 4, the THG response for an irradiance $I = 6 \text{ TW}\cdot\text{cm}^{-2}$ is linear with the number of pulses between 1×10^4 and 5×10^4 pulses. Considering the readout error, the encoding becomes possible with a 16 levels grayscale (4 bits).

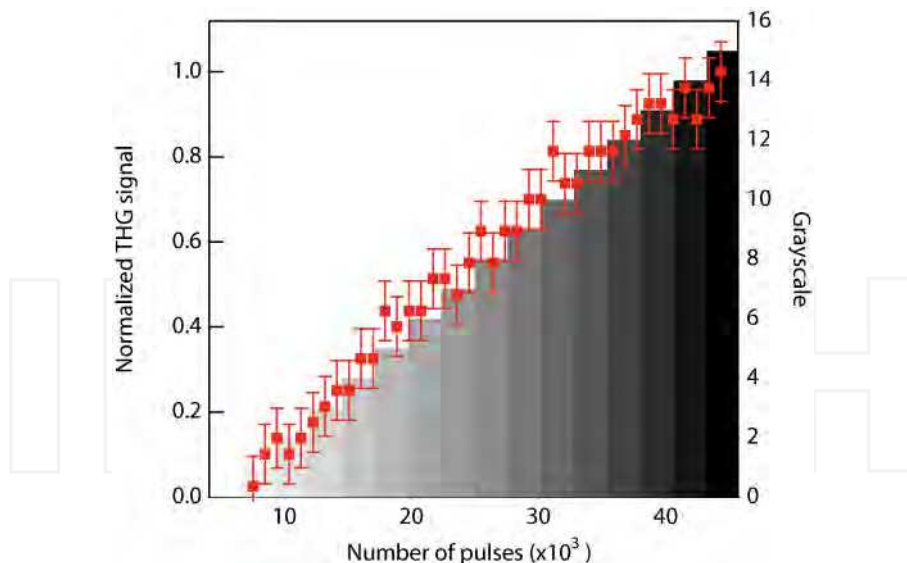


Fig. 5. THG signal versus number of the laser pulses with $I = 6 \text{ TW.cm}^{-2}$. The information can be grayscale encoded.

2.6. 3D optical data storage stability

The photo-written glasses were submitted to different thermal treatments below the transition temperature of the glass $T_g = 375 \text{ }^\circ\text{C}$ at $100 \text{ }^\circ\text{C}$, $200 \text{ }^\circ\text{C}$, $300 \text{ }^\circ\text{C}$, $350 \text{ }^\circ\text{C}$ during 3 h and above T_g at $400 \text{ }^\circ\text{C}$ during 20 min. The THG signal is not modified for temperatures below T_g but disappears for temperatures higher than T_g . The recording is erased only after thermal treatment at $400 \text{ }^\circ\text{C}$ during 20 min corresponding to a total reorganization of the glass. Then, bits could be rewritten inside the glass after polishing. Thus we can state that recording is very stable in standard conditions (up to $85 \text{ }^\circ\text{C}$). In our reading conditions, 10 nJ/pulse , the THG signal is not modified, even after several hours of unstopped exposure (corresponding to 10^{10} readings). Indeed, the Ag clusters are created only if enough photoelectrons are produced (threshold process). This is the reason why no modification appears during the reading process.

2.7. 3D optical data storage capacity

In our experimental conditions (bit spacing, $3 \text{ } \mu\text{m}$; layer spacing, $10 \text{ } \mu\text{m}$), 1 Gbit.cm^{-3} could be stored inside the glass. Better performances can be achieved with a high NA objective ($\text{NA} = 1.4$) even if the objective working distance limits the number of layers. According to Chen & Xie (Chen and Xie, 2002), the THG can reach radial and axial resolutions of 250 nm and 400 nm , respectively. Thus a storage capacity in the range of Tbits.cm^{-3} is possible in the glass. Considering the grayscale encoding, this value can be increased.

3. Spin state transition materials

Spin-crossover systems are a paradigmatic example of bistable optical materials. In such materials, the optical properties can be changed from one state to another through external stimuli such as temperature (T), pressure (P) or light (hv). As the system switches between the two states, its optical properties drastically change in the visible and near IR spectral ranges. These properties were demonstrated in many molecular samples at low temperature. It is only very recently that we have shown that pulsed light irradiations make possible to switch the optical properties of such bistable systems at room temperature. The mechanism responsible for the switching in these particles has also been elucidated. It indicates that less than a thousand photons are required to photo-switch a single nanoparticle of 60 nm in diameter. The offered prospects by such materials in optical and material sciences are therefore very rich and promising.

3.1. Data recording within the hysteresis loop at low temperature

In the last thirty years, the interest in molecular materials that makes possible the storing of a digital information has considerably increased. In such a context, the molecular bistability associated to the spin-crossover (SCO) phenomenon has triggered important research activities. Indeed, the change of the spin state in a SCO material can be induced reversibly in a solid state by adjusting or applying different constraints such as temperature, pressure, light intensity or pulsed magnetic field (Gutlich et al., 1994; Bousseksou et al., 2000). The SCO phenomenon induces for instance an important and reversible change of the optical absorbance or of the magnetic susceptibility of the studied medium. The first photomagnetic effect in an iron(II) SCO material was reported by Decurtins et al. in 1984. At low temperature ($T \leq 50$ K), these authors demonstrated the possibility to convert a compound with a low spin (LS, $S=0$) state into a compound with a metastable high spin (HS, $S=2$) using green light laser beam irradiation. This phenomenon, called Light-Induced Excited Spin-State Trapping (LIESST), was extended later by Hauser, who showed that red light switches the system back to the LS state (reverse-LIESST) (Hauser, 1996). This effect triggered a lot of interest, but most of the published studies have failed to demonstrate the LIESST effect at high temperature. In fact, above 50 K, the photo-induced HS state usually decays within a few minutes. To overcome this limitation, an interesting approach would be to work within the thermal hysteresis loop of a SCO material. Indeed, within the hysteresis loop, both HS and LS states are thermodynamically stable. The first spin change reported in a thermal hysteresis was, in fact, induced using intense magnetic pulses (Bousseksou et al., 2000). However, for practical applications, the use of such external perturbation is not realistic. The first influence of light on a thermal hysteresis loop was described by Renz et al. in 2000. This effect, named Light Perturbed Thermal Hysteresis (LiPTH) was observed under continuous laser irradiation. Depending on the laser wavelength, the hysteresis loop was shifted towards lower temperature or higher temperature. However, the phenomenon relaxes as soon as the laser light is switched-off and considerably limits its application for data storage. Recently, light-induced valence tautomeric conversion was reported in some cobalt-iron Prussian Blue analogs at room temperature (Shimamoto et al., 2002; Liu et al., 2003). It was shown that a single laser pulse converts the electronic state from $\text{Fe}^{\text{II}}(S=0)\text{-CN-Co}^{\text{II}}(S=0)$ to $\text{Fe}^{\text{III}}(S=1/2)\text{-CN-Co}^{\text{II}}(S=3/2)$. The reverse phenomenon has also been observed (Liu et al., 2003). This phenomenon was explained using the so-called domino effect (Koshino & Ogawa, 1998): When the concentration of the local excited HS state is higher than a critical

value, all the system commutes from an LS to an HS state. According to these experiments, one may wonder if a single laser pulse may also induce the same phenomena in a cooperative iron(II) SCO material. To demonstrate it, we have selected the $[\text{Fe}(\text{PM-BiA})_2(\text{NCS})_2]$ (PM-BiA = N-2'-pyridylmethylene-4-aminobiphenyl) complex which exhibits a well defined abrupt hysteresis around 170 K (Létard et al., 1998; Létard et al., 2003). We have shown that, under certain conditions, the use of a single pulse laser in the center of the thermal hysteresis loop leads to a LS \rightarrow HS photo-conversion (Freysz et al., 2004). Compared to the experiments reported on valence tautomeric compounds, our results indicated that the final state reached after a laser excitation is neither a pure HS nor a pure LS state, but it is instead a "mixture" of HS/LS domains. Since the system is firstly photo-excited into the HS state and then slowly relaxes to mixture of HS/LS state, our results cannot be accounted by the so-called domino effect.

The set-up we used to perform these experiments is sketched on Figure 6a. The sample, a powder composed of micro crystallites (a few microns in radius) is sandwiched in between two optical windows and is placed into a cryostat. The specular light reflected by the sample was collected and sent to a 150 mm spectrometer to select the wavelength centered at 600 nm. The resolution of the spectrometer was set to be ~ 2 nm. At the exit of the spectrometer, the light was collected by a photomultiplier connected to a 1 Mega Ohm load. The voltage drop across this load was recorded versus the temperature of the sample in the cryostat. As shown in Figure 6b, this reflection set-up makes possible to record the temperature hysteresis loop of the studied sample. To first record the LS to HS state transitions, the sample is shined with a white light continuum and the light reflected by the sample and transmitted at 600 nm through the spectrometer is recorded by the photo-multiplier. The typical evolution of the reflectivity versus the temperature increase or decrease is presented in Figure 6b. These data are in very good agreement with the measurements performed with a SQUID.

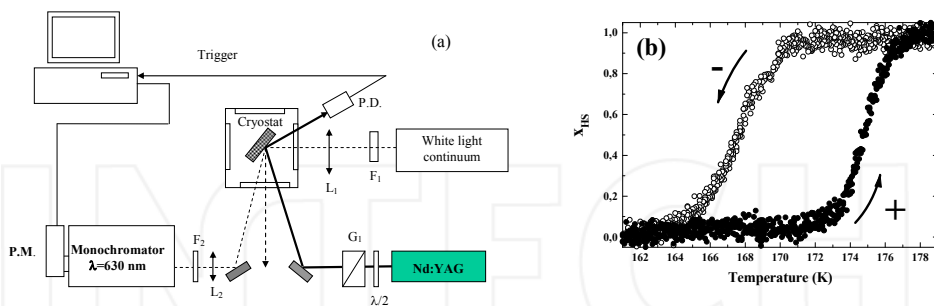


Fig. 6. (a) Sketch of the experimental set-up used to induce and measure the laser induced spin state transition. (b) Evolution of the reflected light versus the temperature. The temperature is either decreased from 180 K to 160 K or increased from 160 K To 180 K. X_{HS} is the molar fraction of molecules in the HS state.

Using this set-up, we have studied the effect of pulsed light on the sample. In this later case, a single laser pulse (Q-switched nanosecond frequency doubled Nd^{3+} :YAG laser, $\lambda_0=0.532$ μm , pulse width 8 ns; energy between 0.5 and 10 mJ) was focused on a spot of about 3 mm

in diameter and only a small fraction of the light reflected by the sample at 600 nm within the laser spot area was imaged and recorded by the spectrometer. As shown in Figure 7a, when the sample is cooled at 140 K, a temperature below the hysteresis loop, we clearly record a temporal evolution of the reflectivity of the sample. According to our calibration, our data clearly show that all the sample probed by the reflected light is brought into the HS state. Moreover, within 0.5 second, it relaxes back to the LS state. By studying the evolution of the HS fraction within the laser spot versus the energy of the laser pulse, we note that the number of HS particles steadily increases versus the energy of the laser pulse up to an energy of ~ 1 mJ. Above 1 mJ, which corresponds to a fluence of $14 \text{ mJ}\cdot\text{cm}^{-2}$ per pulse, all the probed molecules are photo-converted in HS state and the signal saturates. This situation remains until 9 mJ, when a surface photo-degradation of the sample occurs. In conclusion, below the thermal hysteresis and between 78 and 140 K, the photo-induced HS state is not stable. We noted its lifetime decreases from hours (at 60 K) to minutes (at 78 K) and to second (at 140 K) (Degert et al., 2005).

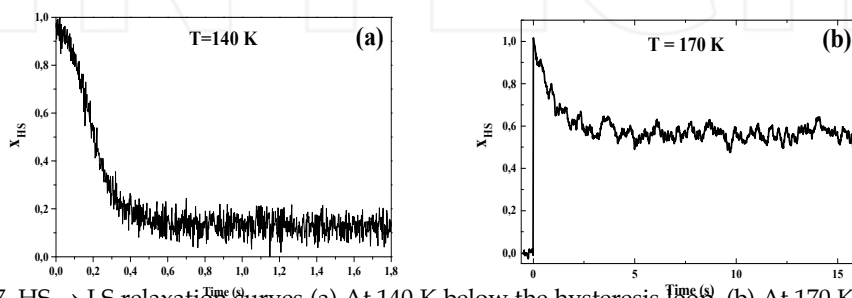


Fig. 7. HS \rightarrow LS relaxation curves (a) At 140 K below the hysteresis loop. (b) At 170 K within the hysteresis loop. The sample was firstly cooled down to a pure LS state and then carefully warmed

Let us now consider the influence of a 1 mJ laser pulse when the sample is set at a temperature within the thermal hysteresis loop. The sample was firstly set into the LS configuration by slowly cooling it and then carefully warming it at $T_1 = 166 \text{ K}$, *i.e.* the region at the beginning of the thermal hysteresis loop. The sample was then excited with a single laser pulse. As reported on Figure 7a, immediately after the single laser pulse, all the probed particles reach the HS state, but they relax back to the LS state. This clearly indicates firstly, that the photo-induced excited HS state is not stable, even within the hysteresis loop and secondly, that the LS \rightarrow HS transition cannot be induced by the photo-excitation of HS molecules. This observation also considerably limits the contribution of a domino effect associated with the excitation of the molecular HS state under our experimental conditions. We then warmed the sample at 170K, *i.e.* the region in the centre of the thermal hysteresis loop, and again excited it with a single laser pulse. Similarly to what reported on Figure 7b, immediately after the single laser pulse, all the probed particles reach the HS state. But this time, they neither relax toward the pure HS state nor the initial LS state. The final situation after relaxation can be regarded as a "mixture" of HS/LS particles. At first, this result is interesting in regard to the opened problem of the thermal effect accompanying the optical excitation of the sample. Indeed, if an artificial and important temperature increase ($\Delta T > 10 \text{ K}$) associated with the absorption of the particles brought the sample in the HS state, it

should, at first glance, remain within this state. This is clearly not the reported experimental result. Moreover, we have also shown that additional laser pulses do not affect the measured HS/LS ratio (Freysz et al., 2004). We have also demonstrated the stability of the photo-induced mixture state within the hysteresis loop. When one steadily increases the temperature of the sample, it remains within this "mixture" state until it reaches the upper and lower temperature branch of the hysteresis loop, respectively labelled $T_{1/2\downarrow}$ and $T_{1/2\uparrow}$. For temperatures higher than $T_{1/2\uparrow}$, all the particles of the sample are converted in the HS state. This latter result demonstrates, if necessary, that the sample is not damaged by the laser pulse. This point was confirmed by the repetition of the experiment many times on the same sample, which did not show any degradation.

Although these experiments were interesting in demonstrating optical data recording in spin state compounds within the hysteresis loop, their practical use was quite limited.

3.2. Data recording within the hysteresis loop and at room temperature

One year after our work, it has been shown that different compounds can be photo-switched at room temperature using a single Nd:YAG Q-switched laser pulse (Bonhommeau et al., 2005). However, the details of the mechanisms giving rise to the switching of the spin state compound within the thermal hysteresis was difficult to evidence (Fouché et al., 2009). In order to investigate these mechanisms, we have carried out an optical study of the SCO complex $[\text{Fe}(\text{NH}_2\text{trz})_3](\text{NO}_3)_2 \cdot 3\text{H}_2\text{O}$ coordination polymer ($\text{NH}_2\text{trz} = 4\text{-amino-1,2,4-triazole}$) known to display a well-defined thermal hysteresis loop at room temperature.

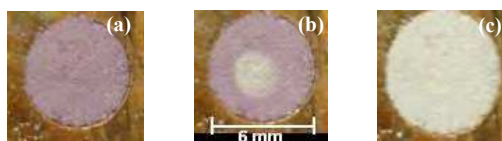


Fig. 8. $[\text{Fe}(\text{NH}_2\text{trz})_3](\text{NO}_3)_2 \cdot 3\text{H}_2\text{O}$ sample in the LS state (a), the HS state (c) and after photo-excitation by a single laser pulse within the hysteresis loop of the compound (b).

As shown in Fig. 8, the colour of the powder, which is pink when the sample is in the LS state (Fig 8a), becomes almost completely white when the sample is in the HS state (Fig. 8c). Indeed, in the LS state, this material displays a broad absorption band at around 520 nm, which is characteristic of the d-d transition of Fe^{2+} (${}^1\text{A}_{1g} \rightarrow {}^1\text{T}_{1g}$), while in the HS state a d-d-transition is recorded at lower energy in the near-infrared region (830 nm). Figure 8b shows the state of the sample impacted by a sequence of pulses yielded by a frequency tripled Nd:YAG laser that delivers pulses at 355nm which duration is $\sim 6\text{ns}$ and fluence on the sample is $E_p \sim 52 \text{ mJ}\cdot\text{cm}^{-2}$. The same experiment has also been performed using pulses with the same fluence but centred at 532 nm. In both cases, we noticed that the central part of the sample impacted by the laser pulse becomes white. The sample remains as it is as long as its temperature is kept within the thermal hysteresis loop. For instance, the whole sample recovers its original pink colour when its temperature is below 10°C . This clearly indicates that within the hysteresis loop, the micro-crystallites of the compound impacted by the laser pulses are brought in the HS state.

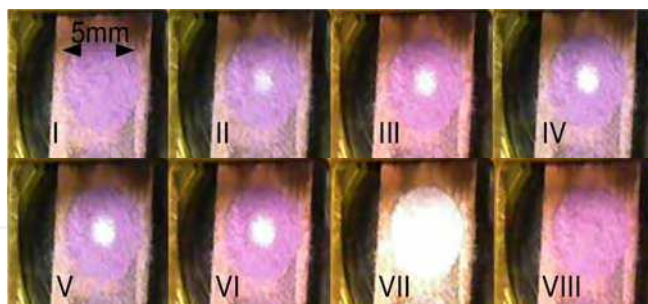


Fig. 9. (I) and (VII) colour of the sample in the LS state. Evolution of the sample set in the thermal hysteresis loop and impacted by (II) one pulse, (III) two pulses, (IV) three pulses, (V) four pulses, (VI) five pulses. (VIII) Colour of the sample impacted by five laser pulse and cooled back in the LS state.

We have also recorded the evolution of the sample versus the laser excitation. Firstly, we noticed that below a certain laser fluence, the sample remains unchanged. Above this threshold fluence, the final state of the compounds depends on both the laser fluence and the number of laser pulses used to excite the sample. As shown in Fig. 9, the central part of the sample shined by the laser beam that is initially in the LS state (I) becomes whiter and whiter as the number of excitation pulses increases (Fig. 9 II to 9 VI). The pictures in Fig. 9VII and 9VIII underline that, for temperature above or below the hysteresis loop, the sample recovers its HS or LS state. This indicates that the sample is not altered by the laser excitation. This experiment also indicates that grayscale encoding is also possible in these materials.

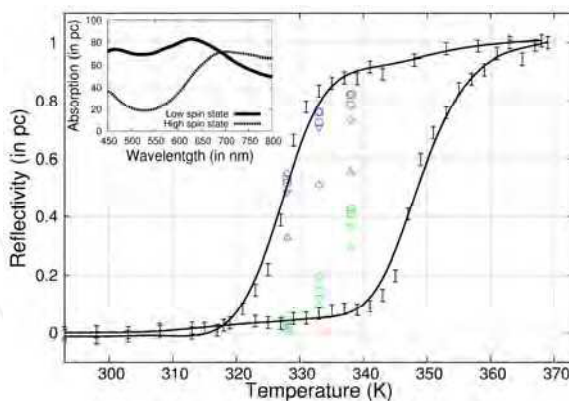


Fig. 10. In solid line: Thermal hysteresis loop deduced from the optical reflectivity and irradiation studies performed at 328 K, 333 K and 338 K by one (Δ), two (∇), three (\circ), four (\square) and five (\diamond) pulses at 355 nm (in blue) and 532 nm (in green) with a fluence of $52 \text{ mJ}\cdot\text{cm}^{-2}$. The inset is the absorption of the powder in the HS and LS states.

To be more quantitative about the final state reached by the sample after each laser pulse, we have replaced the monochromator by a spectrometer and we have recorded the spectrum of the light reflected by the sample after each laser pulse. This enables to fix the state of the sample within the hysteresis loop (Fig. 10). These last data clearly indicate that one can easily perform data recording in this compound. However, they also stress that data recording is easier when the absorption coefficient of the sample is higher. This also clearly underlines that the laser induced heating of the sample is of central importance. To clearly evidence the mechanism responsible for data recording in these materials, we have performed a nanosecond time resolved reflectivity measurement that is described below.

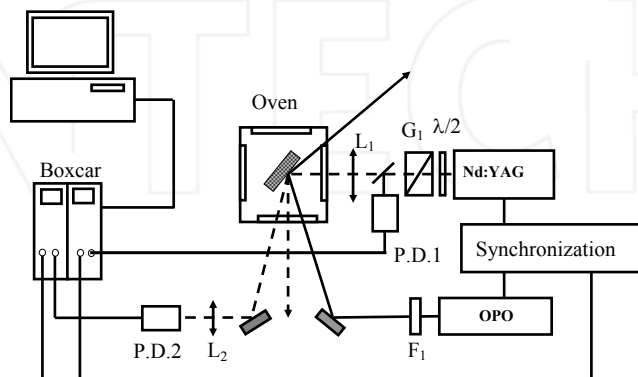


Fig. 11. Nanosecond time resolved pump-probe set-up.

3.2. Kinetic of the data recording

3.2.1. Pump-probe time resolved nanosecond set-up

The optical set-up depicted in Fig. 11 has been designed to record the kinetic of the LS to HS state transition with a nanosecond time resolution. The sample placed in an oven is excited by a "pump" pulse provided by a nanosecond Optical Parametric Oscillator (OPO Panther EX from Continuum), this latter being pumped by a Q-switched-nanosecond-frequency-tripled Nd:YAG laser emitting at $\lambda_0 = 355$ nm (Surelite II from Continuum). The signal and the idler pulses (pulse duration $\tau_{\text{pump}} \sim 6$ ns), produced by a parametric frequency conversion in a type II BBO crystal, are spatially separated by dichroic mirrors. The OPO is tuneable from 400 to 680 nm and from 720 to 2500 nm. At $\lambda_0 = 400$ nm, the maximum pulse excitation energy is ~ 20 mJ. In practice, we adjusted the fluence on the sample by focusing more or less tightly the laser beam. To measure the sample reflectivity change (ΔR) induced by the pump pulse, a "probe" pulse generated by a frequency doubled and Q-switched Nd:YAG laser ($\tau_{\text{probe}} \sim 6$ ns) was used. The probe pulse light diffused by the sample at an angle of 30° was collected by a fast photodiode which output signal is sent in a first boxcar gated integrator. To compensate for pulse to pulse energy fluctuations, the probe pulse reflected by an uncoated optical window placed in front of the sample is used as a reference pulse. It is collected by a second fast photodiode which output signal is connected to a second boxcar gated integrator. The relative sample reflectivity is determined by dividing the signal delivered by the two photodiodes. To control the delay between the pump and probe pulses, the two Nd:YAG lasers are synchronized using a home build-electronic

device. This device, that also delivers the signal that triggers the boxcar gates, makes it possible to temporally delay, from few nanoseconds up to few seconds, the light pulses delivered by these two systems. To limit the impact of OPO fluctuations, we measure the energy of each OPO pulse and only kept the data corresponding to an OPO pulse energy within $\pm 5\%$ of the mean OPO energy value. The signal to noise ratio of our data is further improved by averaging the data over ten laser shots. Finally, to measure the actual reflectivity change of the sample, we record for each pump-probe time delay the relative reflectivity of the sample with and without the pump pulse. In the actual set-up, the sample, a powder composed of micro crystallites a few microns in radius, is sandwiched in between two optical windows and placed into a thermally regulated oven. This set-up has been mainly used when the temperature of the sample is set slightly below the hysteresis loop. In such a case the sample recovers its initial LS state after each pump pulse. Therefore, under these experimental conditions, one records both the formation and the relaxation of the HS fraction induced by the pump pulse.

3.2.2. Experimental results

The reflectivity change ($\Delta R \sim 8\%$) induced by a pump pulse fluence of $E_p \sim 18 \text{ mJ.cm}^{-2}$ is presented in Fig. 12 for a sample at 283 K.

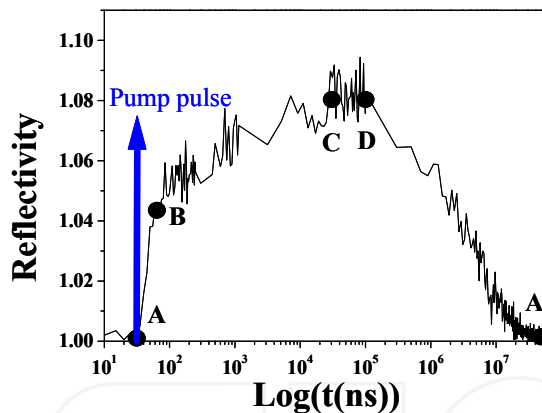


Fig. 13. Time dependence of the reflectivity change at 283 K after photo-excitation with a pump pulse of fluence $E_p \sim 9 \text{ mJ.cm}^{-2}$.

To grasp all the complexity of the dynamic, we have chosen to present our data on a temporal logarithmic scale. Using this scale, one clearly evidences that the growing and the relaxation of the reflectivity is governed by different characteristic times. Figure 12 also indicates that, to register the complete evolution of the system after the pulse excitation, the reflectivity has to be recorded over at least five decades of time. This stresses the advantage of our experimental set-up in which one can adjust continuously the sampling steps along the experiment.

3.2.3. Temporal evolution of the sample within the phase diagram

We have demonstrated that the dynamic of the reflectivity change presented in Fig. 12 can be assigned to respectively:

- The heating of a thin layer (~ 400 nm) of the sample for $0 < t \leq 200$ ns.
- The diffusion of the heat toward the bulk sample and the growing of the HS fraction within the thin layer for $200 \text{ ns} \leq t \leq 100 \mu\text{s}$.
- The relaxation of the HS fraction within the thin layer for $100 \mu\text{s} \leq t \leq 100$ ms.

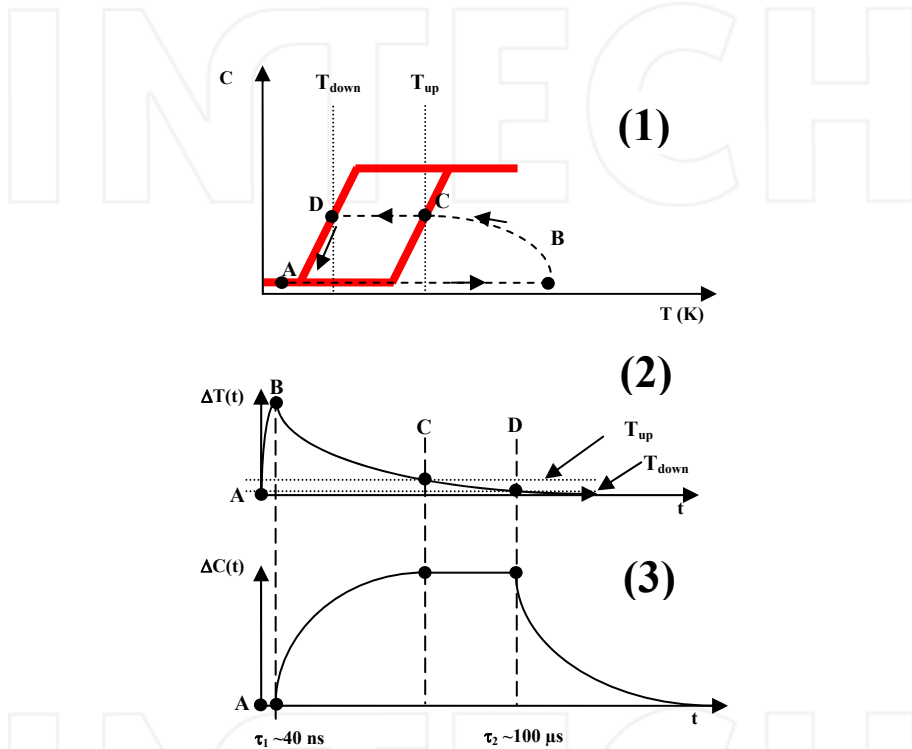


Fig. 14. Mechanisms that account for the laser pulse induced SCO at the vicinity of the thermal hysteresis loop.

As depicted in Fig. 14, this experiment makes also possible to follow the temporal evolution of the sample within the HS concentration, temperature (*i.e.* (C,T) phase diagram of the compound outside the hysteresis loop (Fouché et al., to be published). Upon laser excitation, absorption of the pump energy takes place in a very thin layer L_p (~ 400 nm). As a result, the temperature of this layer increases drastically and is maximum about 40 ns after the laser excitation and sets the sample layer at the point B of the (C,T) diagram. The heat subsequently diffuses toward the bulk sample. Hence, the temperature of the layer steadily decreases so that the sample layer is moving within the phase diagram. The evolution of the HS fraction is less abrupt. During the heating of the layer, it

remains almost constant and then it starts to increase. The growth lasts as long as the temperature of the layer has not reached the ascending branch of the hysteresis loop (point C of the phase diagram). Then, as long as the temperature of the layer remains within the thermal hysteresis loop (*i.e.* between the point C and D of the phase diagram), the HS fraction remains constant. It decreases as soon as the temperature of the layer reaches the descending branch of the hysteresis loop (point D of the phase diagram).

3.2.4. Mechanisms responsible for data recording within the hysteresis loop

The results recorded when the temperature of the sample was set below the hysteresis loop and presented in the previous section makes possible to understand the evolution of the sample when its temperature is set within the hysteresis loop as depicted in Fig.9. Figure 15 shows the evolution of the sample after each laser pulse.

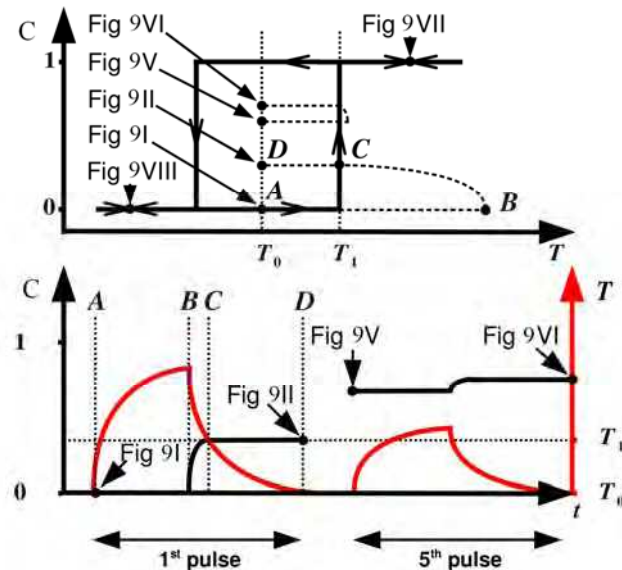


Fig. 15. Path in the phase diagram followed by the sample after each laser shot and evolution of the temperature (grey line) and the HS fraction (black line) of the sample after each laser shot.

At first, just after the laser excitation, the absorption of the pulse by a thin layer of the sample induces a local heating. Within a hundred of nanoseconds, the absorbed energy heats the system; its temperature rises up very quickly at a temperature where the LS state is unstable. The higher the absorption coefficient is, the higher the temperature increase is. Thus the sample is thermally quenched (A → B), whereas only a very small HS fraction appears. Then, the sample cools and an increase of the HS fraction takes place (B → C). As shown in Fig. 14, this process lasts about 100 μ s. Once the ascending branch of the hysteresis loop is reached, the HS fraction no longer evolves and the created HS fraction coexists with the LS fraction. Finally, the powder reaches the temperature of the oven (C → D). The whole

process takes about 1 ms. The sample has then reached a state where its absorption coefficient decreases. Indeed, as shown in inset of the Fig. 10, the absorption of the sample in the HS state is reduced at both 532 nm and 355 nm. Thus, for the subsequent laser pulses, the laser induced heating is less and less important, the growth lasts less and less time and the increase of the HS fraction is less and less important. After a few pulses, the sample has reached a state located within the thermal hysteresis loop (Fig. 14). In the last case, one can further improve the LS to HS conversion efficiency by increasing the laser pulse energy. Based on this scenario, the highest efficiency recorded at 355 nm is directly accounted by the highest absorption of the sample in the blue spectral range (inset of Fig. 10), leading to a greater heating of the sample.

3.3. Future and prospects

Our on going study deals with bistable nanoparticles with controlled sizes, shapes and optical properties. Such particles offer many prospect for data recording. Our computations indicate that less than a thousand of photons are required to photo-switch a single nanoparticle of 60 nm in diameter. On the other hand, we are also performing experiments that make possible to understand and to master the physical mechanisms responsible for the photo-switching of these nanoparticles inserted in different controlled polymeric environments. We are also currently testing their practical uses for holographic data recording.

4. References

- Barille, R.; Canioni, L.; Sarger, L. & Rivoire, G. (2002). Nonlinearity measurements of thin films by third-harmonic-generation microscopy, *Phys. Rev. E*, 66, 067602
- Belharouak, I.; Parent, C.; Tanguy, B.; Le Flem, G. & Couzy, M. (1999). Silver aggregates in photoluminescent phosphate glasses of the 'Ag₂O-ZnO-P₂O₅' system, *J. Non-Cryst. Solids.*, 244, 238-249
- Bellec, M.; Royon, A.; Bousquet, B.; Bourhis, K.; Treguer, M.; Cardinal, T.; Richardson, M. & Canioni, L. (2009), Beat the diffraction limit in 3D direct laser writing in photosensitive glass, *Opt. Exp.*, 17, 10304-10318
- Bousseksou, A.; Negre, N.; Goiran, M.; Salmon, L.; Tuchagues, J.P.; Boillot, M.L.; Boukheddaden, K. & Varret, J. F. (2000), Dynamic triggering of a spin-transition by a pulsed magnetic field, *Eur. Phys. J. B*, 13, 451
- S. Bonhommeau, G. Molnar, A. Galet, A. Zwick, J.A. Real, J.J. McGarvey & A. Bousseksou (2005), One-Shot-Laser-Pulse-Induced Reversible Spin Transition in the Spin Crossover Complex {Fe(C₄H₄N₂)[Pt(CN)₄]} at Room Temperature, *Angew. Chem. Int. Ed.*, 44 4069
- Brocas, A.; Canioni, L. & Sarger, L. (2004). Efficient selection of focusing optics in non linear microscopy design through THG analysis, *Opt. Exp.*, 12, 2317-2322
- Canioni, L.; Bellec, M.; Royon, A.; Bousquet, B. & Cardinal, T. (2008). Three-dimensional optical data storage using third-harmonic generation in silver zinc phosphate glass. *Opt. Lett.*, 33, 360-362
- Chen, J. & Xie, S. (2002). Green's function formulation of third-harmonic generation microscopy, *J. Opt. Soc. Am. B*, 19, 1604

- Dai, Y.; Hu, X.; Wang, C.; Chen, D.; Jiang, X.; Zhu, C.; Yu, B. & Qiu, J. (2007). Fluorescent Ag nanoclusters in glass induced by an infrared femtosecond laser, *Chem. Phys. Lett.*, 439, 81
- Day, D. & Gu, M. (1998). Effects of Refractive-Index Mismatch on Three-Dimensional Optical Data-Storage Density in a Two-Photon Bleaching Polymer, *Appl. Opt.*, 37, 6299-6304
- Decurtins, S.; Gütllich, P.; Köhler, C.P.; Spiering, H. & Hauser, A. (1984), Light-induced excited spin state trapping in a transition-metal complex: The hexa-1-propyltetrazole-iron (II) tetrafluoroborate spin-crossover system, *Chem. Phys. Lett.*, 105, 1-4.
- Degert, J.; Lascoux, N.; Montant, S.; Létard, S.; Freysz, E.; Chastanet, G. & Létard, J.-F. (2005), Complete temperature study of the relaxation from the high-spin state to low-spin state in a strongly cooperative spin crossover compound, *Chem. Phys. Lett.* 415, 206-210
- Dmitryuk, A. V.; Paramzina, S. E.; Perminov, A. S.; Solov'eva, N. D. & Timofeev, N. T. (1996). The influence of glass composition on the properties of silver-doped radiophotoluminescent phosphate glasses, *J. Non-Cryst. Solids*, 202, 173-177
- Fouché, O.; Degert, J.; Jonusauskas, G.; Baldé, C.; Desplanche, C.; Létard, J.-F. & Freysz, E. (2009), Laser induced spin state transition: Spectral and temporal evolution, *Chem. Phys. Lett.*, 469, 274-278
- Freysz E, Montant S, Letard S & Létard J.F. (2004), Single laser pulse induces spin state transition within the hysteresis loop of an Iron compound, *Chem. Phys. Lett.*, 394, 318-323
- Jiu, H.; Tang, H.; Zhou, J.; Xu, J.; Zhang, Q.; Xing, H.; Huang, W. & Xia, A. (2005). Sm(DBM)3Phen-doped poly(methylmethacrylate) for three-dimensional multilayered optical memory, *Opt. Lett.*, 30, 774-776
- Gütllich, P.; Hauser, A. & Spiering, H. (1994), Thermal and Optical Switching of Iron(II) Complexes, *Angew. Chem. Int. Ed. Engl.*, 33, 2024-2054
- Hauser, A. (1986), Reversibility of light-induced excited spin state trapping in the Fe(ptz)6(BF4)2, and the Zn_{1-x}Fe_x(ptz)6(BF4)2 spin-crossover systems, *Chem. Phys. Lett.* 124, 543-548
- Jones, H. D. & Reiss, H. R. (1977). Intense-field effects in solids, *Phys. Rev. B*, 16, 2466-2473
- Keldysh, L. V. (1965). Ionization in the field of a strong electromagnetic wave, *Sov. Phys. JEPT*, 20, 1307-1314
- Koshino, K. & Ogawa, T (1998), Domino effects in photoinduced structural change in one-dimensional systems, *J. Phys. Soc. Jap.* 67, 2174
- Létard, J.-F.; Guionneau, P.; Rabardel, L.; Howard, J. A. K.; Goeta, A. E.; Chasseau, D. & Kahn, O. (1998), Structural, Magnetic, and Photomagnetic Studies of a Mononuclear Iron(II) Derivative Exhibiting an Exceptionally Abrupt Spin Transition. Light-Induced Thermal Hysteresis Phenomenon, *Inorg. Chem*, 37, 4432-4441
- Létard, J.-F.; Chastanet, G.; Nguyen, O.; Marcen, S.; Marchivie, M.; Guionneau, P.; Chasseau, D.; Gütllich, P. (2003), Spin Crossover Properties of the [Fe (PM-BiA) 2 (NCS) 2] Complex-Phases I and II, *Monatshefte für Chemie* 134, 165
- Li, X.; Bullen, C.; Chon, J. W. M.; Evans, R. A. & Gu, M. (2007). Two-photon-induced three-dimensional optical data storage in CdS quantum-dot doped photopolymer, *Appl. Phys. Lett.*, 90, 161116

- Liu, H.W.; Matsuda, K.; Gu, Z.Z.; Takahashi, K.; Cui, A.L.; Nakajima, R.; Fujishima, A. & Sato, O. (2003), Reversible Valence Tautomerism Induced by a Single-Shot Laser Pulse in a Cobalt-Iron Prussian Blue Analog, *Phys. Rev. Lett.* 90, 167403
- Mok, F. K. (1993). Angle-multiplexed storage of 5000 holograms in lithium niobate, *Opt. Lett.*, 18, 915-917
- Pan, S.; Shih, A.; Liou, W.; Park, M.; Bhawalkar, J.; Swiatkiewicz, J.; Samarabandu, J.; Prasad, P. N. & Cheng, P. C. (1997). *Scanning* 19, 156
- Psaltis, D.; Levene, M.; Pu, A. & Barbastathis, G. (1995). Holographic storage using shift multiplexing, *Opt. Lett.*, 20, 782-784
- Rakuljic, G. A.; Leyva, V. & Yariv, A. (1992). Optical data storage by using orthogonal wavelength-multiplexed volume holograms, *Optics Letters*, 17, 1471-1473
- Renz, F.; Spiering, H.; Goodwin, H.A. & Gütllich, P (2000), Light-perturbed hysteresis in an iron (II) spin-crossover compound observed by the Mössbauer effect, *Hyperfine Interactions* 126, 155
- Schneckenburger, H.; Regulla, D. F. & Unsöld, E. (1981). Time-resolved investigations of radiophotoluminescence in metaphosphate glass dosimeters, *Appl. Phys. A*, 26, 23-26
- Shen, Y. R. (1984). *The Principles of Nonlinear Optics*, Wiley
- Squier, J. & Muller, M. (1999). Third-harmonic generation imaging of laser-induced breakdown in glass, *Appl. Opt.*, 38, 5789-5794
- Strickler, J. H. & Webb, W. W. (1991). Three-dimensional optical data storage in refractive media by two-photon point excitation, *Opt. Lett.*, 16, 1780-1782
- Stuart, B. C.; Feit, M. D.; Herman, S.; Rubenchik, A. M.; Shore, B. W. & Perry, M. D. (1996). Nanosecond-to-femtosecond laser-induced breakdown in dielectrics, *Phys. Rev. B*, 53, 1749-1761
- Sun, H. B.; Tanaka, T.; Takada, K. & Kawata, S. (2001). Finer features for functional microdevices, *Nature*, 412, 697-698
- Shimamoto, N.; Ohkoshi, S.-S.; Sato, O. & Hashimoto, K. (2002), One-Shot-Laser-Pulse-Induced Cooperative Charge Transfer Accompanied by Spin Transition in a Co-Fe Prussian Blue Analog at Room Temperature, *Chem. Lett.*, 31, 486

INTECH

INTECH



Data Storage

Edited by Florin Balasa

ISBN 978-953-307-063-6

Hard cover, 226 pages

Publisher InTech

Published online 01, April, 2010

Published in print edition April, 2010

The book presents several advances in different research areas related to data storage, from the design of a hierarchical memory subsystem in embedded signal processing systems for data-intensive applications, through data representation in flash memories, data recording and retrieval in conventional optical data storage systems and the more recent holographic systems, to applications in medicine requiring massive image databases.

How to reference

In order to correctly reference this scholarly work, feel free to copy and paste the following:

Matthieu Bellec, Lionel Canioni, Arnaud Royon, Bruno Bousquet, Jerome Degert, Eric Freysz, Thierry Cardinal and Jean-Francois Letard (2010). Optical Data Storage in Photosensitive Glasses and Spin State Transition Compounds, Data Storage, Florin Balasa (Ed.), ISBN: 978-953-307-063-6, InTech, Available from: <http://www.intechopen.com/books/data-storage/optical-data-storage-in-photosensitive-glasses-and-spin-state-transition-compounds>

INTECH

open science | open minds

InTech Europe

University Campus STeP Ri
Slavka Krautzeka 83/A
51000 Rijeka, Croatia
Phone: +385 (51) 770 447
Fax: +385 (51) 686 166
www.intechopen.com

InTech China

Unit 405, Office Block, Hotel Equatorial Shanghai
No.65, Yan An Road (West), Shanghai, 200040, China
中国上海市延安西路65号上海国际贵都大饭店办公楼405单元
Phone: +86-21-62489820
Fax: +86-21-62489821